Regioregular Head-to-Tail Oligothiophene-Functionalized 9,9'-Spirobifluorene Derivatives. 2. NMR Characterization, Thermal Behaviors, and Electrochemical Properties

Jian Pei,*,[†,‡] Jing Ni,[‡] Xing-Hua Zhou,[†] Xiao-Yu Cao,[†] and Yee-Hing Lai[‡]

College of Chemistry and Molecular Engineering, Peking University, Beijing 100871, People's Republic of China, and Institute of Materials Research and Engineering and Department of Chemistry, National University of Singapore, Singapore 117602

jianpei@chem.pku.edu.cn

Received June 11, 2002

Oligothiophene-functionalized 9,9'-spirobifluorene derivatives exhibit good solubility in polar organic solvents, especially compounds **5a**−**d** to **7a**−**d** due to the introduction of the flexible *n*-hexyl chain. The structures of all compounds studied are characterized and verified by ^{1}H and ^{13}C NMR spectra. The results not only show that these organic conjugated materials with no substituents or *n*-hexyl substituents are successfully synthesized through the corresponding synthetic methodologies, but also prove that chemical shifts of protons and carbons in the aromatic range change with the attachment and the increase of the thiophene ring at the 9,9'-spirobifluorene fragment. The thermal analysis results demonstrate that these compounds are quite stable, and evaporate from 300 to 700 °C. Most of these compounds exhibit a stable amorphous state in the solid state. The electrochemical properties of all compounds studied are also investigated. The results indicate that radical cation behaviors of oligothiophene-modified 9,9'-spirobifluorene derivatives are more stable than those of normal oligothiophenes, that oxidative and reductive peak potentials shift cathodically or anodically, and that the HOMO and LUMO energy levels are also tuned with the increase of the thiophene ring owing to the enhanced π-electron delocalization and the increasing conjugation length. Oxidative potentials of nonsubstituted oligothiophene-functionalized 9,9'-spirobifluorene derivatives are more sensitive to the increase of thiophene rings than those of 9,9'-spirobifluorene derivatives with *n*-hexyl groups. The energy levels and band gaps of all compounds studied are also calculated from the onset potentials of n-doping and p-doping and are adjusted by varying thiophene oligomers and their attachment patterns to the 9,9'-spirobifluorene ring to make them suitable for the work functions of the electrodes.

Introduction

Organic conjugated materials (low molecular weight materials, oligomers, and polymers) have attracted considerable interest due to their potential applications toward photonic and optoelectronic displays in the past two decades.[1] The purification and the thermal stability of organic materials in the solid state are often required to avoid problems associated with grain boundaries present in polycrystalline materials, especially for the fabrication of electroluminescent (EL) devices. Most of the organic conjugated materials with low molecular weights generally tend to crystallize readily; hence, they usually exist as crystals below their melting points, which prevents them from forming amorphous glasses at ambient temperature.[2] The tendency to spontaneously crystallize presents a limitation in use for organic EL devices because the crystal formation destroys film homogeneity, and crystal boundaries raise the resistance of the sample, eventually leading to electrical-shorting.[3] Therefore, most recently, considerable effort has been made to produce organic low molecular weight conjugated compounds as good amorphous glasses in the solid state.

As the thermodynamic nonequilibrium state needs to form stable amorphous glasses above room temperature, amorphous molecular materials may form uniform, transparent amorphous thin films by vapor deposition or spin-coating, and also exhibit isotropic properties as well as homogeneous properties. Furthermore, in comparison with polymers, they not only are pure materials with well-defined molecular structures and definite molecular weight without distributions, but also have better con-

---

* To whom correspondence should be addressed. Fax: 86-10-62751708.
† Peking University.
‡ National University of Singapore.

(1) (a) *Handbook of Conducting Polymers*, 2nd ed.; Skotheim, T. A., Ed.; Dekker: New York, 1997. (b) *Conjugated Conducting Polymers*; Kies, H., Ed.; Springer: Berlin, 1992; Vol. 102. (c) *Conjugated polymers*; Brédas, J. L., Sylbey, R., Eds.; Kluwer: Dordrecht, The Netherlands, 1991. (d) Miller, J. S. *Adv. Mater.* **1993**, *5*, 671. (e) Kanatzidis, M. G. *Chem. Eng. News* **1990**, 36. (f) Roncali, J. *Chem. Rev.* **1992**, *92*, 711. (g) Kraft, A.; Grimsdale, A. C.; Holmes, A. B. *Angew. Chem., Int. Ed.* **1998**, *37*, 402.

(2) (a) Plazek, D. J.; Magill, J. H. *J. Chem. Phys.* **1966**, *45*, 3038. (b) Greet, R. J.; Turnbull, D. *J. Chem. Phys.* **1966**, *46*, 1243.
(3) Joswick, M. D.; Campbell, I. H.; Barashkov, N. N.; Ferraris, J. P. *J. Appl. Phys.* **1996**, *80*, 2883.

SCHEME 1.   Chemical Structures of 9,9′-Spirobifluorene Derivatives
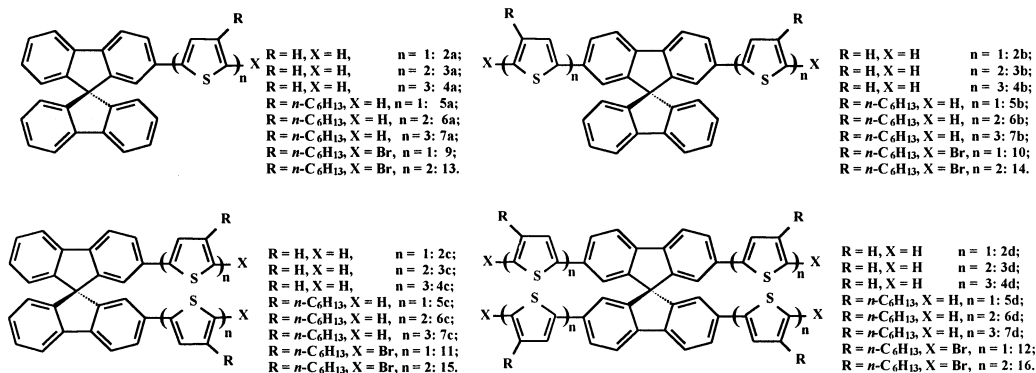
trolled structures without generation of structural defects normally existing in polymers.

Among these approaches to create amorphous molecules suitable for use in photoelectronic devices, especially for use in electroluminescent devices, creating nonplanar molecular structure seems very effective. The investigation of the relationship between the molecular structure and the glass-forming property and stability has provided several approaches to prepare amorphous molecular materials, including a number of π-electron starburst molecules,[4] dendritic macromolecules,[5] tetrahedral-shaped molecules,[6] spiro-linked compounds based on π-electron systems,[7] and other compounds.[8] Among these materials, the specific, orthogonally fused structure, such as the spiro-type molecules, entitles them the desired steric demand, which minimizes the interchain contacts of the molecules, and hence prevents crystallization.

In our previous paper, we reported the synthesis of a series of oligothiophene-functionalized 9,9′-spirobifluorene derivatives through the Negishi and the Suzuki coupling reactions in high yields (as shown in Scheme 1).[9] We also collated the differences of the yields in the preparation of thiophione-functionalized 9,9′-spirobifluorene derivatives employing these two coupling methods. Herein, we present the ^{1}H and ^{13}C NMR characterization of some desired compounds to understand the effect of the conjugation of materials on the NMR spectra. We discuss the effect of the substituents at the thiophione ring on the thermal stability and the amorphous state of these molecules. Moreover, we also exhibit interesting electrochemical properties of oligothiophene-functionalzed 9,9′-spirobifluorenes to further understand the effect of sp³-hybrid carbon at the spiro center on the whole molecule.

(4) (a) Bettenhausen, J.; Strohriegl, P. *Adv. Mater.* **1996**, *8*, 507. (b) Shirota, Y.; Kobata, T.; Noma, N. *Chem. Lett.* **1989**, 1145.

(5) (a) Wang, P. W.; Liu, Y. J.; Devadoss, C.; Bharathi, P.; Moore, J. S. *Adv. Mater.* **1996**, *8*, 237. (b) Louie, J.; Hartwig, J. F.; Fry, A. J. *J. Am. Chem. Soc.* **1997**, *119*, 11695.

(6) Wang, S.; J. Oldham, W. J.; Hudack, J. R. A.; Bazan, G. C. *J. Am. Chem. Soc.* **2000**, *122*, 5695.

(7) (a) Salbeck, J.; Yu, N.; Bauer, J.; Weissörtel, F.; Bestgen, H. *Synth. Met.* **1997**, *91*, 209. (b) Salbeck, J.; Weissörtel, F.; Bauer, J. *Macromol. Symp.* **1998**, *125*, 121.

(8) (a) Naito, K.; Miura, A. *J. Phys. Chem.* **1993**, *97*, 6240. (b) Naito, K. *Chem. Mater.* **1994**, *6*, 2343.

(9) Pei, J.; Ni, J.; Zhou, X.-H.; Cao, X.-Y.; Lai, Y.-H. *J. Org. Chem.* **2002**, *67*, 4924.

Experimental Section

^{1}H and ^{13}C NMR spectra were collected using chloroform-*d* as the solvent and tetramethylsilane (TMS) as the internal standard. Thermogravimetric analysis (TGA) was conducted under a heating rate of 10 °C/min from room temperature to 800 °C with an air flow of 75 cm³/min. Differential scanning calorimetry (DSC) was run under a heating rate of 20 °C/min and a nitrogen flow rate of 70 cm³/min. Cyclic voltammetry (CV) of all derivatives was conducted at a potential scan rate of 40 mV/s under an argon atmosphere. All potentials were measured in a three-electrode cell with a 0.1 mol/L solution of tetrabutylammonium hexylfluorophosphate (n-Bu$_4$NPF$_6$) as the electrolyte, using a Ag/Ag$^+$ electrode (0.1 M AgNO$_3$ in acetonitrile) as the reference electrode (0.34 V vs SCE), a platinum wire as the counter electrode, and a platinum disk (effective area 0.5−1.0 cm²) coated by a thin layer of a molecular compound as the working electrode. All experimental values were corrected with respect to SCE.

Results and Discussion

^{1}H and ^{13}C NMR Characterization. Although oligothiophenes without substitutents usually exhibit poor solubility in common organic solvents, the introduction of a 9,9′-spirobifluorene fragment with steric demand greatly improved the solubility and processability of our desired compounds. Unsubstituted oligothiophene-functionalized 9,9′-spirobifluorene derivatives were readily dissolved in polar organic solvents, including THF and chloroform. After the introduction of *n*-hexyl groups into the thiophene ring, these 9,9′-spirobifluorene derivatives showed good solubility in common solvents such as hexane, chloroform, THF, DMF, and xylene.

For example, the ^{1}H NMR chemical shifts and assignments of protons in the aromatic range of compounds **2a**−**4a** are summarized in Table 1. ^{1}H NMR spectra of compounds **1a**, **3a**, **1b**, and **3b** are shown as representatives in Figure 1. For compound **1a**, we observed that the slightly different local electron environments of H-7, H-2′, and H-7′ (about δ 7.10 ppm), H-6, H-3′, and H-6′ (about δ 7.35 ppm), and H-4, H-5, H-4′, and H-5′ (about δ 7.85 ppm) afforded poorly resolved multiple peaks. However, for compound **3a**, the doublet peaking at about δ 6.70 ppm with a coupling constant of 7.6 Hz corresponded to H-8 of the 9,9′-spirobifluorene ring, and another doublet at δ 6.76 ppm with coupling constants of 0.8 and 7.6 Hz was assigned to H-1′ and H-8′. The two doublets centered at about δ 7.60−7.63 ppm with coupling constants of 2.0 and 8.0 Hz resulted from H-3. We also observed that, in comparison with those of compound

TABLE 1. ^{1}H NMR Chemical Shifts in the Aromatic Range for Compounds 1a−4a (ppm)

2a: n = 1;
3a: n = 2;
4a: n = 3

protons	1a	2a	3a	4a
H-1	6.85 (d)	7.06 (s)	6.93−6.94 (d)	6.94 (s)
H-8	6.71−6.74 (m)	6.78−6.80 (d), J = 7.6 Hz	6.70−6.72 (d), J = 7.6 Hz	6.70−6.72 (d), J = 7.6 Hz
H-1′,8′	6.71−6.74 (m)	6.84−6.87 (dd), J = 0.8, 7.6 Hz	6.76−6.79, J = 0.8, 7.6 Hz	6.76−6.79, J = 7.6 Hz
H-7,2′,7′	7.08−7.17 (m)	7.14−7.20 (m)	7.08−7.13 (m)	7.08−7.15 (m)
H-3	7.48−7.50 (dd), J = 1.6, 7.6 Hz	7.70−7.72 (dd), J = 1.6, 7.6 Hz	7.60−7.63 (dd), J = 1.6, 7.6 Hz	7.60−7.64 (dd), J = 1.6, 7.6 Hz
H-6,3′,6′	7.34−7.41 (m)	7.40−7.47 (m)	7.34−7.41 (m)	7.37−7.41 (m)
H-4,5,4′,5′	7.69−7.71 (d), 7.80−7.86 (m)	7.89−7.95 (m)	7.82−7.90 (m)	7.83−7.89 (m)
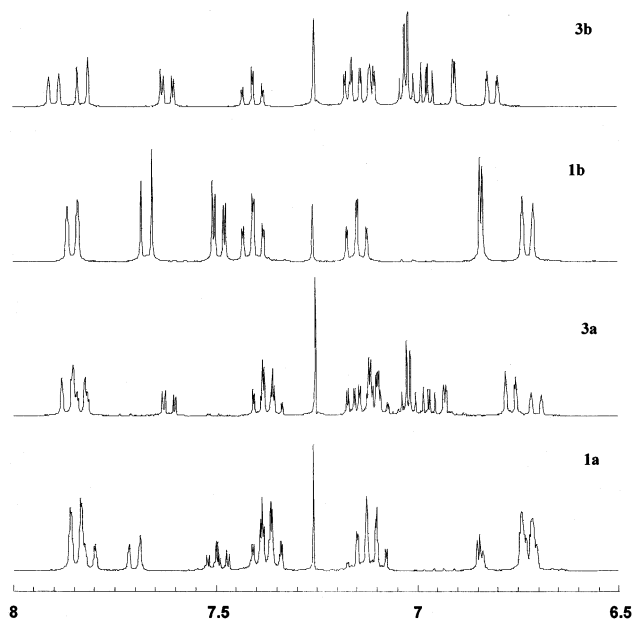
FIGURE 1. ^{1}H NMR spectra in the aromatic range for compounds **1a**, **1b**, **3a**, and **3b**.

1a, the chemical shifts of the protons of compound **3a** moved downfield from about δ 6.85 ppm to δ 6.93−6.94 ppm for H-1, from δ 7.49 ppm to δ 7.63 ppm for H-3, from δ 7.70 ppm to δ 7.82−7.90 ppm for H-4, owing to the increased π-electron delocalization and conjugation length of the whole molecule after more thiophene rings attached at the phenyl ring.
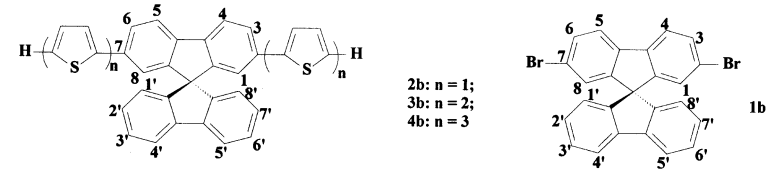
The ^{1}H NMR chemical shifts and assignments of protons in the aromatic range of compounds **2b**−**4b** are also summarized in Table 2. For compound **3b**, the doublet centered at δ 6.92 ppm was assigned to H-1 and H-8. The doublet peaking at about δ 6.80−6.83 ppm with a coupling constant of 7.2 Hz was assigned to H-1′ and H-8′. The two doublets at δ 7.61−7.64 ppm with coupling constants of 1.6 and 8.0 Hz corresponded to H-3 and H-6. The three doublets located within δ 7.38−7.44 ppm were attributed to H-3′ and H-6′. The doublets centered at δ 7.82−7.90 ppm were assigned to protons at the 4,5- and 4′,5′-positions. H-2′ and H-7′ were assigned to the multiplets ranging from δ 7.11 ppm to δ 7.18 ppm. We also observed that chemical shifts of most protons, except those at the 2′,3′,6′,7′-positons of compound **3b**, moved

downfield. For example, in comparison with those of compound **1b**, the chemical shifts of the protons of compound **3b** moved downfield from δ 6.71 ppm to δ 6.80 ppm for H-1′ and H-8′, from δ 6.83−6.84 ppm to δ 6.92 ppm for H-1 and H-8, from δ 7.48 ppm to δ 7.64 ppm for H-3 and H-6, and from δ 7.67 ppm to δ 7.83 ppm for H-4 and H-5, also attributed to the increased π-delocalization and conjugation length of the whole molecule after more thiophene rings attached at the 9,9′-spirobifluorene system. For the assignments and rules the protons at the 9,9′-spirobifluorene ring of compounds **2c**−**4c** and **2d**−**4d** were very similar to those of compounds **2a**−**4a** and **2b**−**4b**. For all protons on the 9,9′-spirobifluorene ring of compounds **2a**−**d** to **4a**−**d**, the chemical shifts moved downfield in comparison with the corresponding protons of starting materials **1a**−**d**, which was due to the enhancement of the increased π-electron delocalization and conjugation after the attachment of thiophene rings.
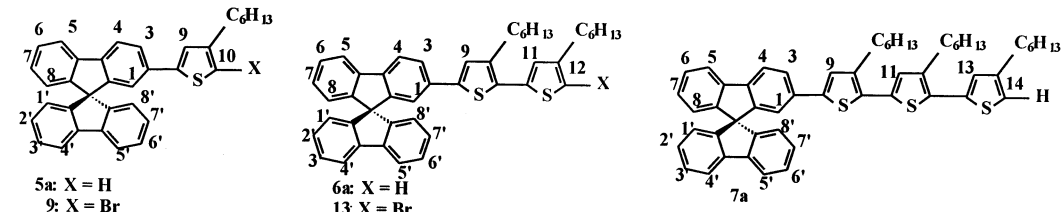
The chemical shifts and assignments of protons in the aromatic region of compounds **5a**−**7a** and their corresponding bromide intermediates **9** and **13** are listed in Table 3, and ^{1}H NMR spectra in the aromatic range are shown in Figure 2. For 3-*n*-hexylthiophene-functionalized 9,9′-spirobifluorene derivatives **5a**−**7a**, ^{1}H NMR spectra in the aromatic range exhibited similar couplings, splittings, and changes in comparison with compounds **2a**−**4a** with an increase of thiophene rings in comparison with **1a**. For compound **5a**, two doublet peaks at δ 6.75 and 6.94 ppm with a very small coupling constant (1.2 Hz) belonged to H-9 and H-10 of the thiophene ring, respectively. The coupling constant was much lower than the coupling constant of normal α-H and β-H (about 5.2 Hz) of the thiophene ring, which resulted from the resonance of α-H (H-9) and γ-H (H-10).[10,11] It indicated that the C−C bond formation between the aromatic group and 5-position of the 3-*n*-hexylthiophene ring was carried out through the Suzuki coupling reactions between

(10) (a) Pelter, A.; Jenkins, I.; Jones, D. E. *Tetrahedron* **1997**, *53*, 10357. (b) Zotti, G.; Salmaso, R.; Gallazzi, M. C.; Marin, R. A. *Chem. Mater.* **1997**, *9*, 791. (c) Welzel, H.-P.; Kossmehl, G.; Boettcher, H.; Engelmann, G.; Hunnius, W.-D. *Macromolecules* **1997**, *30*, 7419. (d) Li, W.; Maddux, T.; Yu, L. *Macromolecules* **1996**, *29*, 7329.

(11) (a) Pei, J.; Yu, W.-L.; Ni, J.; Lai, Y.-H.; Huang, W.; Heeger, A. L. *Macromolecules* **2001**, *34*, 7421. (b) Yu, W.-L.; Huang, W.; Heeger, A. J. *Macromolecules* **2000**, *33*, 2462. (c) Pei, J.; Yu, W.-L.; Huang, W.; Heeger, A. J. *Chem. Commun.* **2000**, 1631. (d) Liu, B.; Yu, W.-L.; Lai, H.-Y.; Huang, W. *Macromolecules* **2000**, *33*, 8945. (e) Pei, J.; Yu, W.-L.; Huang, W.; Heeger, A. J. *Synth. Met.* **1999**, *105*, 43. (f) Pei, J.; Yu, W.-L.; Huang, W.; Heeger, A. J. *Acta Polym.* **1999**, *50*, 327.

TABLE 2. ¹H NMR Chemical Shifts in the Aromatic Range for Compounds 1b–4b (ppm)

2b: n = 1;
3b: n = 2;
4b: n = 3

1b

protons	1b	2b	3b	4b
H-1,8	6.83−6.84 (d), $J = 1.6$ Hz	6.93 (d), $J = 1.6$ Hz	6.92 (d), $J = 1.6$ Hz	6.91 (d), $J = 1.6$ Hz
H-1′,8′	6.71−6.74 (d), $J = 7.6$ Hz	6.80−6.82 (d), $J = 7.6$ Hz	6.80−6.83 (d), $J = 7.6$ Hz	6.80−6.82 (d), $J = 7.6$ Hz
H-2′,7′	7.12−7.18 (td)	7.11−7.17 (m)	7.11−7.18 (m)	7.12−7.21 (m)
H-3,6	7.47−7.51 (dd), $J = 1.6, 8.0$ Hz	7.62−7.65 (dd), $J = 1.6, 8.0$ Hz	7.61−7.64 (dd), $J = 1.6, 8.0$ Hz	7.61−7.63 (dd), $J = 1.6, 8.0$ Hz
H-3′,6′	7.38−7.43 (td), $J = 1.2, 7.6$ Hz	7.37−7.42 (td), $J = 1.2, 7.6$ Hz	7.38−7.44 (td), $J = 1.2, 7.6$ Hz	7.39−7.44 (t), $J = 7.2$ Hz
H-4,5	7.66−7.68 (d), $J = 8.0$ Hz	7.82−7.84 (d), $J = 8.0$ Hz	7.82−7.84 (d), $J = 8.0$ Hz	7.82−7.85 (d), $J = 8.0$ Hz
H-4′,5′	7.85−7.87 (d), $J = 7.6$ Hz	7.87−7.90 (d), $J = 7.6$ Hz	7.88−7.91 (d), $J = 7.6$ Hz	7.89−7.92 (d), $J = 7.6$ Hz

TABLE 3. ¹H NMR Chemical Shifts and Assignments in the Aromatic Region of Compounds 5a–7a, 9, and 13 (ppm)

5a: X = H
9: X = Br

6a: X = H
13: X = Br

7a

| protons	5a	9	6a	13	7a
H-1	6.96−6.97 (d), $J = 1.6$ Hz	6.89−6.90 (d), $J = 1.6$ Hz	6.95−6.96 (d), $J = 1.6$ Hz	6.92−6.93 (d), $J = 1.6$ Hz	6.93 (s)
H-8	6.69−6.72 (d), $J = 7.6$ Hz	6.71−6.74 (d), $J = 7.6$ Hz	6.70−6.73 (d), $J = 7.6$ Hz	6.70−6.72 (d), $J = 7.6$ Hz	6.71−6.74 (d), $J = 7.6$ Hz
H-1′	6.76−6.79 (d), $J = 7.6$ Hz	6.77−6.79 (dd), $J = 7.6$ Hz	6.78−6.80 (d), $J = 7.6$ Hz	6.77−6.79 (dd), $J = 7.6$ Hz	6.79−6.82 (d), $J = 7.6$ Hz
H-7,2′	7.05−7.15 (m)	7.09−7.16 (m)	7.08−7.16 (m)	7.08−7.15 (m)	7.09−7.17 (m)
H-3	7.60−7.63 (dd), $J = 1.6, 8.0$ Hz	7.52−7.55 (dd), $J = 1.6, 8.0$ Hz	7.61−7.64 (dd), $J = 1.6, 8.0$ Hz	7.59−7.62 (dd), $J = 1.6, 8.0$ Hz	7.62−7.65 (d), $J = 8.0$ Hz
H-6,3′	7.34−7.42 (m)	7.35−7.43 (m)	7.34−7.42 (m)	7.34−7.42 (m)	7.35−7.43 (m)
H-4,5,4′	7.82−7.89 (m)	7.82−7.90 (m)	7.83−7.90 (m)	7.82−7.90 (m)	7.84−7.91 (m)
H-9	6.75−6.76 (d), $J = 1.4$ Hz	6.83 (s)	6.97 (s)	6.95 (s)	6.99 (s)
H-10	6.94−6.95 (d), $J = 1.4$ Hz				
H-11			6.85−6.86 (d), $J = 1.2$ Hz	6.76 (s)	6.97 (s)
H-12			6.91−6.92 (d), $J = 1.2$ Hz		
H-13					6.89 (s)
H-14					6.97 (s)

2-bromo-9,9′-spirobifluorene and sodium 4-*n*-hexyl-2-thienylboronate, and also further demonstrated that sodium 4-hexyl-2-thienylboronate was successfully prepared despite the high selectivity of lithiation at the 5-position of 3-*n*-hexylthiophene by use of LDA. The same results were verified in our previous papers.[11] In comparison with the ¹H NMR spectrum of compound **5a**, for its bromide derivatives **9**, we observed that the doublet with low coupling constant peaking at about δ 6.75−6.76 ppm belonging to H-9 of the thiophene ring moved downfield and became a sharp singlet peak at about δ 6.83 ppm. However, another doublet at δ 6.97 ppm (H-1) and a doublet−doublet resonance at δ 7.63 ppm (H-3) moved upfield owing to the bromination of the thiophene ring. Of course, the doublet belonging to H-10 disappeared. We also found that the multipeaks from about δ 6.75 ppm to δ 6.80 ppm split into two parts, one of which moved downfield as the doublet peak with low coupling constant (1.6 Hz) and the other of which had slight alternation. After one more thiophene ring was attached to convert compound **9** into compound **6a**, in the ¹H NMR spectrum of compound **6a**, we observed that the resonance moving upfield in the spectrum of compound **9** shifted downfield again due to the increased π-electron density and conjugation length. For instance, the singlet peak corresponding to H-9 moved downfield at δ 6.97 ppm and the doublet−doublet peaks at about δ 7.52 ppm moved downfield at δ 7.62 ppm. Moreover, two new doublet peaks with a small coupling constant of 1.2 Hz appeared at δ 6.85 and 6.91 ppm, which resulted from H-11 and H-12 of the second thiophene ring, respectively. The same results were observed again in the spectra of the corresponding bromide **13** of compound **6a**, and one more thiophene ring coupling derivative **7a** of compound **13**.

For other *n*-hexyl-substituted thiophene-functionalized 9,9′-spirobifluorene derivatives **5b−d** to **7b−d** and their corresponding bromides **10−12** and **14−16**, the ¹H NMR spectra also exhibited alternations and rules similar to those of compounds **5a−7a**. Table 4 shows the ¹H NMR chemical shifts and assignments in the aromatic range of compounds **5b−7b**, **10**, and **14**.

¹³C NMR spectra were also employed to further verify the structure of desired compounds. The ¹³C NMR chemical shifts and assignments in the aromatic range of compounds **5b−7b** and their corresponding bromides **10** and **14** are summarized in Table 5, and ¹³C NMR spectra in the aromatic range are illustrated in Figure 3. For
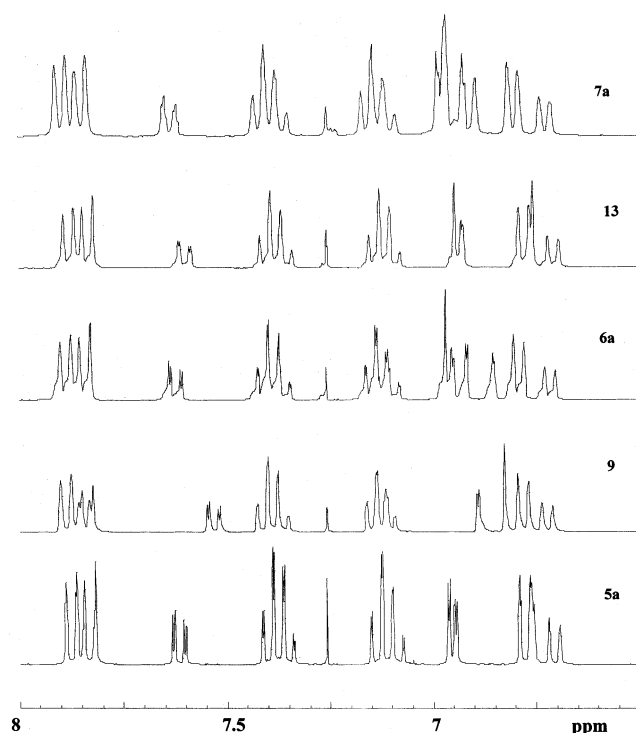
FIGURE 2. ¹H NMR spectra in the aromatic region of compounds **5a**, **6a**, **7a**, **9**, and **13**.
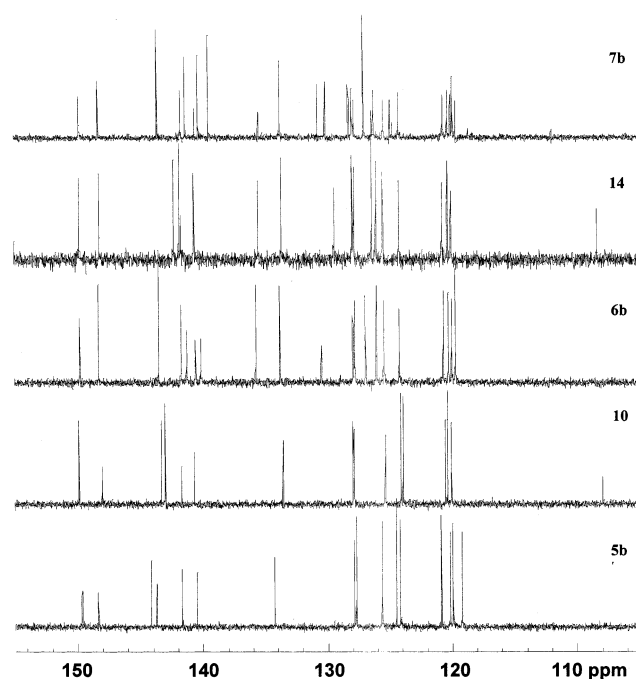
FIGURE 3. ¹³C NMR spectra of compounds **5b**, **6b**, **7b**, **10**, and **14** in the aromatic region.

compound **5b**, the chemical shift of the end α-C was located at 119.3 ppm, which moved upfield to around 108 ppm for compound **10** after bromination of the thiophene ring. The coupling reaction of one more thiophene ring attaching to C-10 of compound **10** reconverted the C–Br bond to a C–C linkage, which caused a downfield shift of about 33 ppm to 141.3 ppm. The chemical shift of the end α-C of compound **6b** appeared at 119.7 ppm, similar
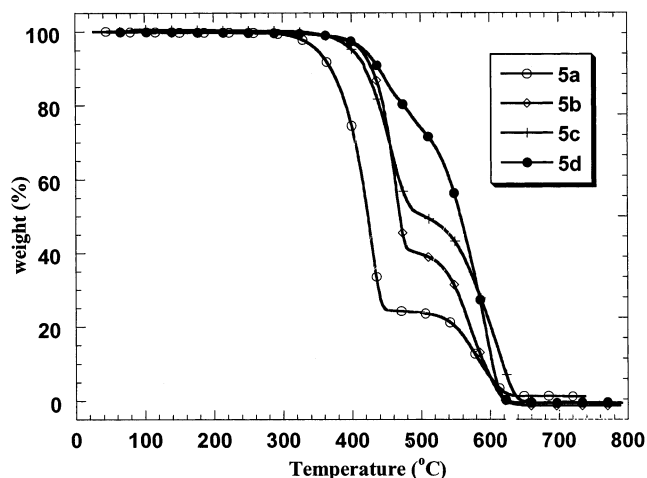
**FIGURE 4.** TGA chart of compounds **5a–d** in air at a heating rate of 10 °C/min.

to that of compound **5b**, which moved upfield to around 108.3 ppm after the bromination again. After the attachment of the third thiophene ring to compound **14** occurred, the chemical shift moved downfield to around 139 ppm. ¹³C NMR spectra of other *n*-hexyl-substituted thiophene-functionalized 9,9′-spirobifluorene derivatives and their corresponding bromides were also identical as above.

Thermal Analysis. For the photoelectronic application, the thermal stability of organic materials is critical for device stability and lifetime. The degradation of organic photoelectronic devices depends on morphological changes resulting from the thermal instability of the amorphous organic layer.[12] The morphological change might be promoted by the rapid molecular motion near the glass transition temperature (T_g). Therefore, it is obvious that the development of organic materials with high T_g is a fundamental task to improve the thermal stability of organic materials and the device lifetime. The thermal and morphologic stability of oligothiophene-fuctionalized 9,9′-spirobifluorene derivatives was measured by using TGA and DSC.

Table 6 summarizes the onsets of evaporation and temperatures of glass transition (T_g) and crystallization (T_c) and melting points (T_m) of all derivatives **2a–d** to **7a–d**. It indicated that all these compounds exhibited an onset of evaporation or decomposition greater than 280 °C with no weight loss at lower temperature. The TGA chart of compounds **5a–d** is shown in Figure 4 as an example. The evaporation of the four compounds onset at about 295, 375, 359, and 345 °C, respectively. Additionally, this chart also demonstrated that the thermal stability of these materials improved with the increase of thiophene rings at the 9,9′-spirobifluorene systems.

Compounds **2a–d** to **4a–d**, 9,9′-spirobifluorene derivatives without substituents, exhibited high glass transition temperatures (>100 °C) and were in an amorphous state at room temperature. We observed that compounds **2a**, **2c**, **2d**, **3a**, **3c**, **4b**, and **4d** formed kinetically stable amorphous phases after thermal annealing. These com-

(12) (a) Kagan, J.; Arora, S. K. *J. Org. Chem.* **1983**, *48*, 4317. (b) Han, E. M.; Do, L. M.; Niidome, Y.; Fujihira, M. *Chem. Lett.* **1994**, 969.

TABLE 4. ¹H NMR Chemical Shifts and Assignments in the Aromatic Region of Compounds 5b−7b, 10, and 14 (ppm)
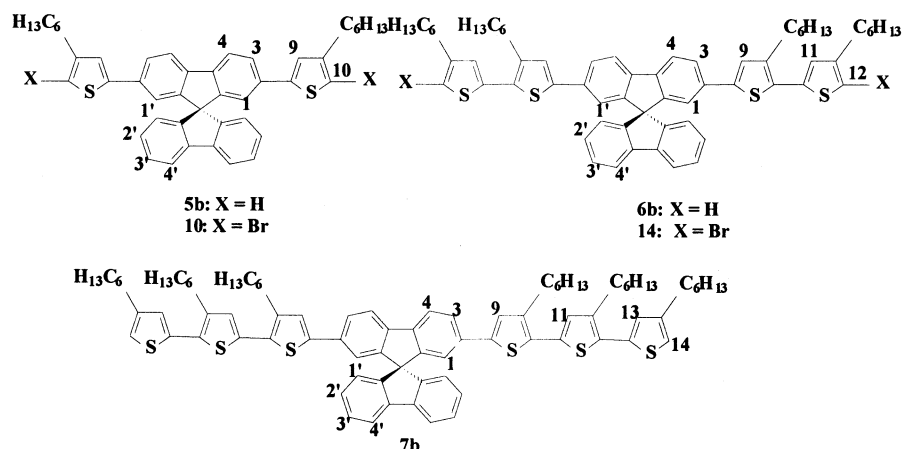
protons	5b	10	6b	14	7b
H-1	6.90−6.91 (d), $J = 1.6$ Hz	6.81−6.82 (d), $J = 1.6$ Hz	6.90−6.91 (d), $J = 1.6$ Hz	6.88−6.89 (d), $J = 1.6$ Hz	6.96−6.97 (d), $J = 1.6$ Hz
H-1′	6.80−6.83 (dd), $J = 1.2, 7.6$ Hz	6.77−6.80 (d), $J = 7.6$ Hz	6.83−6.80 (m)	6.80−6.83 (d), $J = 7.6$ Hz	6.83−6.86 (d), $J = 7.6$ Hz
H-2′	7.11−7.17 (td), $J = 1.1, 7.6$ Hz	7.11−7.16 (t), $J = 7.6$ Hz	7.12−7.17 (t), $J = 7.6$ Hz	7.12−7.17 (td), $J = 1.1, 7.6$ Hz	7.14−7.19 (t), $J = 7.6$ Hz
H-3	7.62−7.65 (dd), $J = 1.6, 8.0$ Hz	7.49−7.52 (dd), $J = 1.6, 8.0$ Hz	7.60−7.62 (dd), $J = 1.6, 8.0$ Hz	7.58−7.61 (dd), $J = 1.6, 8.0$ Hz	7.61−7.64 (dd), $J = 1.6, 8.0$ Hz
H-3′	7.37−7.42 (td), $J = 1.1, 7.6$ Hz	7.39−7.44 (t), $J = 7.6$ Hz	7.39−7.44 (t), $J = 7.6$ Hz	7.39−7.44 (td), $J = 1.1, 7.6$ Hz	7.41−7.46 (t), $J = 7.6$ Hz
H-4	7.80−7.82 (d), $J = 8.0$ Hz	7.79−7.81 (d), $J = 8.0$ Hz	7.80−7.83 (d), $J = 8.0$ Hz	7.80−7.83 (d), $J = 8.0$ Hz	7.81−7.84 (d), $J = 8.0$ Hz
H-4′	7.89−7.91 (d), $J = 7.6$ Hz	7.88−7.90 (d), $J = 7.6$ Hz	7.90−7.92 (d), $J = 7.6$ Hz	7.90−7.92 (d), $J = 7.6$ Hz	7.92−7.94 (d), $J = 7.6$ Hz

TABLE 5. ¹³C NMR Chemical Shifts and Assignments in the Aromatic Region of Compounds 5b−7b, 10, and 14 (ppm)

carbons	5b	10	6b	14	7b
carbons at the spirobifluorene ring	149.7	149.9	149.8	149.8	149.8
	148.4	148.0	148.3	148.2	148.3
	141.7	141.7	141.7	141.7	141.7
	140.5	140.7	140.6	140.6	140.6
	134.3	133.6	133.8	133.6	133.7
	127.9	128.0	128.0	128.0	128.0
	127.7	127.9	127.8	127.8	127.8
	125.7	125.4	126.0	126.0	126.2
	124.5	124.1	125.4	125.5	125.5
	124.2	124.0	124.2	124.2	124.2
	120.9	120.6	120.7	120.7	120.7
	120.2	120.4	120.3	120.3	120.3
C-10	119.3	108.0	141.3	141.8	141.4
C-12			119.7	108.3	139.4
C-14					119.9

TABLE 6. TGA and DSC Data for All Compounds Studied

compd	onset of decomposition (TGA, °C)	T_g (DSC, °C)	T_c (DSC, °C)	T_m (DSC, °C)
2a	286	133.5	b	b
2b	287	119.0	154.7	281.2
2c	314	161.0	b	b
2d	353	186.0	b	b
3a	307	101.0	b	b
3b	388	127.3	173.6	282.7
3c	394	130.2	b	b
3d	390	161.0	229.1	297.4
4a	344	104.0	181.4	218.7, 245.4
4b	464	163.0	b	b
4c	420	127.8	230.5	304.1
4d	397	184.2	b	b
5a	295	a	b	b
5b	375	205.2	b	b
5c	359	a	b	b
5d	345	a	b	b
6a	305	a	b	b
6b	386	a	b	b
6c	358	164.9	b	b
6d	330	a	b	b
7a	303	a	b	b
7b	310	133.2	b	b
7c	337	a	b	b
7d	373	a	b	b

ᵃ No obvious glass transition on heating the sample. *ᵇ* No crystallization and melting on heating the sample.

pounds were initially obtained as microcrystalline powders when precipitated from solutions. Accordingly pristine samples typically showed a weak and broad melting endothermic peak on the first heating cycle of the DSC experiment. Once residual solvents in the samples were removed, only the amorphous phases of most of the compounds were observed, and no recrystallization and melting peaks were observed upon heating above the glass transition temperature (T_g); however, other compounds, **2b**, **3b**, **3d**, **4a**, and **4c**, exhibited obvious crystallization and melting behavior above the glass transition temperature. Typical differential scanning calorimetry thermogram characteristics of compound **2b** are shown in Figure 5 for elucidation.

While the polycrystalline sample, compound **2b**, obtained by recrystallization from CHCl₃/EtOH, was heated in the first run, a sharp endothermic peak due to the

melting curve maximized at 293.7 °C. When the isotropic liquid was cooled on standing in liquid nitrogen, a transparent glass film was spontaneously formed via the supercooled liquid. When the amorphous glass sample was heated again in the second run, a glass transition phenomenon, where the specific heat and other physical properties changed, was observed at 119.0 °C. On further
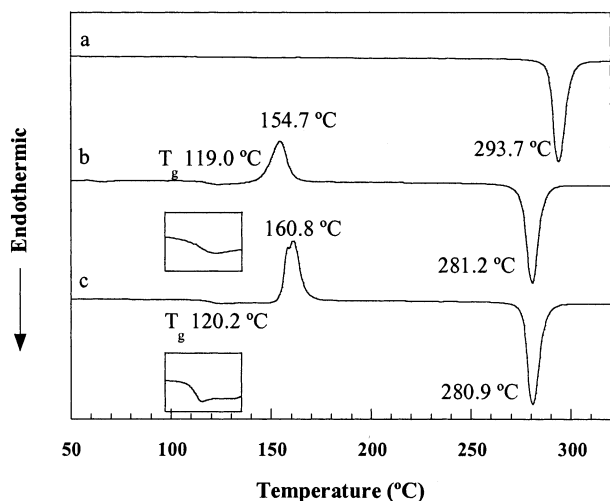
FIGURE 5. DSC curves of compound **2b**: (a) first run; (b) second run; (c) third run.

FIGURE 6. DSC curves (second run) of compound **4a**.

heating above the glass transition temperature (T_g), an exothermic peak due to the crystallization was observed at 154.7 °C to form crystals, which melted at 281.2 °C again. In the subsequent third run, the sample showed the same behavior as in the second run. Similar thermal behavior was also found for some new families of amorphous molecular materials, such as 4,4′,4″-tris[3-methylphenyl(phenyl)amino]triphenylamine,[4b] spirosexiphenyl,[13] and 2,2′,7,7′-tetrakis(diphenylamino)-9,9′-spirobifluorene.[14]

DSC analysis of compound **3b** gave sharp recrystallization and melting peaks similar to those of compound **2b**, with the only difference being the characteristic temperature value. For compounds **3d** and **4d**, which have different attachment patterns to the 9,9′-spirobifluorene, the recrystallization peaks were weaker and broader than those of compounds **3b** and **4b**. This might be due to their different behaviors of the crystallization process and relate to their molecular shapes resulting from the different attachment patterns to the 9,9′-spirobifluorene ring. This was further proved by the DSC thermogram results for compound **4a**. Noteworthy was that compound **4a** was found to exhibit polymorphism, assuming different crystalline forms depending upon the history of heat treatment. Figure 6 shows the DSC thermogram of compound **4a**. During the first heating run, the crystalline sample of **4a** exhibited the same behavior upon heating as **2b**, and an endothermic signal due to melting was observed peaking at 243.6 °C. When the isotropic liquid was rapidly cooled with liquid nitrogen, a transparent glass film also formed. When the amorphous glass was again heated, an obvious glass transition was observed at 104.0 °C, and then an exothermic peak due to crystallization to form crystal A was observed around 181.4 °C, which was followed by two endothermic peaks. All characterization results demonstrated that the appearance of two endothermic peaks could not be caused by impurities existing in the compound. We attributed the first endothermic peak at 218.7
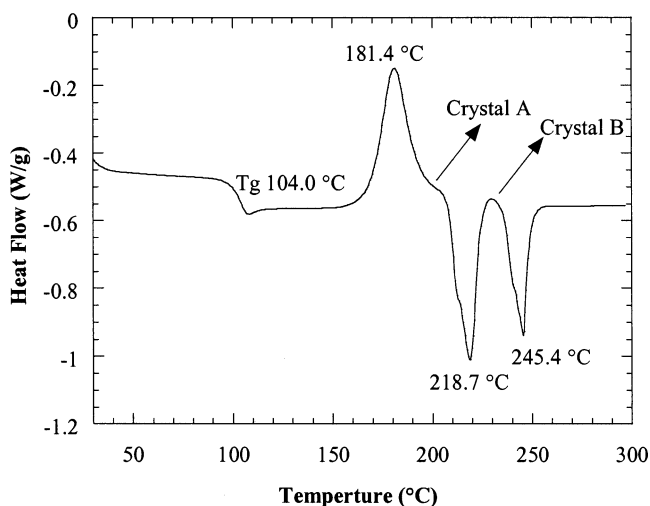
°C to a solid−solid phase transition, where crystal A was transformed into a different crystal form (crystal B). The second endothermic peak at 245.4 °C was due to the melting of crystal B upon further heating. It was reported that 1,3,5-tris[4-methylphenyl(phenyl)amino]benzene (p-MTDAB), 1,3,5-tris[2-thienyl(phenyl)amino]benzene(α-TPTAB), and 1,3,5-tris[3-thienyl(phenyl)amino]benzene (β-TPTAB) underwent similar solid−solid phase transitions involving melting or crystallization or both.[15]

As we know, nonsubstituted α-oligothiophenes naturally intend to crystallize, and single crystals have grown to the octathiophenes (α-8T) with the exception of α-septithiophene (α-7T).[16] In contrast, our oligothiophene-functionalized 9,9′-spirobifluorene derivatives **2a−d** to **4a−d** without substituents were found to easily form amorphous glasses at ambient temperature due to the introduction of the 9,9′- spirobifluorene system. They exhibited high morphological stability with high glass transition temperatures ranging from 101 to 186 °C, as summarized in Table 6. The results showed that compounds **2a−d** to **4a−d** were stable enough to be used as electroluminescent materials, photovoltaic materials, photochromic resist materials, and other photoelectronic materials, and also demonstrated that the introduction of 9,9′-spirobifluorene was an effective structural modification to obtain a high glass transition temperature.

In comparison with compounds **2a−d** to **4a−d**, no obvious glass transition was observed for most compounds of the H−T regioregular oligothiophene-functionalized 9,9′-spirobifluorene derivatives, with the exception of compounds **5b**, **6c**, and **7b**, which possessed high glass transition temperatures of 205.2, 164.9, and 133.2 °C, respectively. For these compounds, no crystallization and/

(13) Steuber, F.; Staudigel, J.; Stössel, M.; Simmerer, J.; Winnacker, A.; Spreitzer, H.; Weissörtel, F.; Salbeck, J. Adv. Mater. **2000**, 12, 130.
(14) Ishikawa, W.; Inada, H.; Nakado, H.; Shirota, Y. Mol. Cryst. Liq. Cryst. **1992**, 211, 431.

(15) (a) Ishikawa, W.; Inada, H.; Nakano, H.; Shirota, Y. Chem. Lett. **1991**, 1731. (b) Ueta, E.; Nakano, H.; Shirota, Y. Chem. Lett. **1994**, 2397. (c) Nakano, H.; Ueta, E.; Shirota, Y. Mol. Cryst. Liq. Cryst. **1998**, 313, 241.
(16) (a) Chaloner, P. A.; Hitchcock, P. B.; Gunatunga, S. R. Acta Crystallogr. **1994**, C50, 1941. (b) van Bolhuis, F.; Wynberg, H.; Havinga, E. E.; Meijer, E. W.; Staring, E. G. J. Synth. Met. **1989**, 30, 381. (c) Porzio, W.; Destri, S.; Mascherpa, M.; Bruckner, S. Acta Polym. **1993**, 44, 266. (d) Horowitz, G.; Bachet, B.; Yassar, A. Lang. P.; Demanze, F.; Fave, J. L.; Garnier, F. Chem. Mater. **1995**, 7, 1337. (e) Fichou, D.; Bachet, B.; Demanze, F.; Billy, I.; Horowitz, G.; Garnier, F. Adv. Mater. **1996**, 8, 500.

TABLE 7. p-Doping and n-Doping Characteristics of All Compounds Studied

	p-doping			n-doping			energy level (eV)		band gap (eV)
	E_{onset}	E_{pa}	E_{pc}	E_{onset}	E_{pc}	E_{pa}	HOMO	LUMO	
2a	1.24	1.44		−1.67	−2.14		5.63	2.72	2.91
		1.69							
2b	1.10	1.60		−1.72	−2.23		5.49	2.67	2.82
2c	1.23	1.54		−1.70	−2.10		5.62	2.69	2.93
		1.87							
2d	1.20	1.45		−1.62	−2.23	−2.29	5.59	2.77	2.82
					−2.33				
3a	0.90	1.00	0.69	−1.90	−2.17	−2.23	5.29	2.49	2.80
		1.13	0.85						
		1.25	1.06						
3b	0.84	1.26	1.12	−1.65	−2.10	−1.70	5.23	2.74	2.49
3c	0.81	1.20	0.99	−1.71	−1.98	−1.66	5.20	2.68	2.52
3d	0.86	1.15	0.97	−1.53	−1.71		5.25	2.86	2.39
4a	0.87	1.08	0.54	−1.55	−2.00		5.26	2.84	2.42
			0.93						
4b	0.68	0.92	0.93	−1.50	−1.73		5.07	2.89	2.18
					−1.96				
4c	0.68	1.02	0.90	−1.60	−1.99		5.07	2.79	2.28
					−2.18				
4d	0.65	0.93	0.88	−1.55	−1.96	−1.59	5.04	2.84	2.20
5a	1.05	1.21		−1.83	−2.18		5.44	2.56	2.88
5b	0.92	1.12	0.88	−1.90	−2.17	−2.02	5.31	2.49	2.82
5c	1.00	1.09	0.98	−1.98	−2.50		5.39	2.41	2.98
5d	0.99		1.08	−1.90	−2.39		5.38	2.49	2.89
6a	0.94	1.08	0.99	−1.80	−2.33		5.33	2.59	2.74
6b	0.80	1.00	0.75	−1.65	−2.15		5.19	2.74	2.45
			0.95						
6c	0.93	1.08	0.91	−1.74	−2.10		5.32	2.65	2.67
6d	0.88	1.03	0.89	−1.55	−1.97		5.27	2.84	2.43
7a	0.75	0.84	0.60	−1.55	−1.81		5.14	2.84	2.30
					−2.59				
7b	0.82	0.94	0.80	−1.45	−1.88		5.21	2.94	2.27
7c	0.89	0.96	0.81	−1.45	−1.92		5.28	2.94	2.34
7d	0.85	0.98	0.81	−1.49	−2.06		5.24	2.90	2.34

or melting process was observed upon heating to 300 °C, while it was observed in a few end- and side-substituted oligothiophene (α-nT) derivatives.[17] The results demonstrated that crystallization tendency was significantly reduced and thus the morphology stability was improved for compounds **5a**−**d** to **7a**−**d** in comparison with substituted oligothiophenes, which also was attributed to the introduction of steric demand by 9,9′-spirobifluorene, preventing the close and regular stacking and packaging of molecules required for crystal growth. Recrystallization is responsible for the significant reduction of fluorescence quantum efficiencies of oligothiophenes from solutions to film states, as well as for device degradation by destroying film homogeneity and raising the resistance of the layer, eventually leading to electrical-shorting.[3] Hence, the significantly reduced crystallization tendency of H−T regioregular compounds with *n*-hexyl groups was expected to enhance the photoluminescence efficiencies in comparison with those of their parent alkyl-substituted oligothiophenes.

The specific, orthogonally fused structure of the spiro-type molecules entitles them the desired steric demand, which minimizes interchain contacts of the molecules and hence prevents crystallization. The ability to form a molecular glass and to reduce the crystallization tendency of the resulting molecules and consequently to prevent the crystal boundaries has been widely demonstrated.

Electrochemical Properties. The redox data and the HOMO and LUMO energy levels calculated from the onset potentials of p-doping and n-doping in cyclic voltammetry are listed in Table 7. Although cyclic voltammograms of oligothiophene-functionalized 9,9′-spirobifluorene derivatives showed some characteristics similar to those reported for oligothiophenes and poly-thiophenes, such as good reversibility of the p-doping process with a relatively broad width at half-height (PWHH),[18] most of the derivatives showed very clear redox behaviors upon anodic scan which were different from those of common oligothiophenes, in which peaks corresponding to dimers, monocations, dications, and even trications were often observed.[19] It indicated that radical cation behaviors of oligothiophene-modified 9,9′-spirobifluorene derivatives were more stable than those of normal oligothiophenes. However, a few compounds, including compounds **2a**, **2c**, **3a**, **3b**, and **3c**, still showed peaks and bumps corresponding to dimer formation and/or dications. Two oxidative peaks were exhibited for compounds **2a** (about 1.44 and 1.69 V) and **2c** (about 1.54 and 1.87 V), which corresponded to the radical cations and dications, respectively. The swelling before the first peak was attributed to the oxidation of formed dimers, which was also observed for compounds **3b** and **3c**. For compound **3a**, three well-resolved oxidative peaks and

(17) (a) Hotta, S.; Waragai, K. *J. Mater. Chem.* **1991**, *1*, 835. (b) Liao, J. H.; Benz, M.; LeGoff, E.; Kanazidis, M. G. *Adv. Mater.* **1994**, *6*, 135. (c) Azumi, R.; Gotz, G.; Bauerle, P. *Synth. Met.* **1999**, *101*, 544.

(18) (a) Marque, P.; Roncali, J.; Garnier, F. *J. Electoanal. Chem.* **1987**, *218*, 107. (b) Hubbard, A. T.; Anson, F. C. *Anal. Chem.* **1966**, *38*, 1887. (c) Laviron, E. *J. Electroanal. Chem.* **1972**, *39*, 1.

(19) Barth, M.; Guilerez, S.; Bidan, G.; Bras, G.; Lapkowski, M. *Electrochim. Acta* **2000**, *45*, 4409.
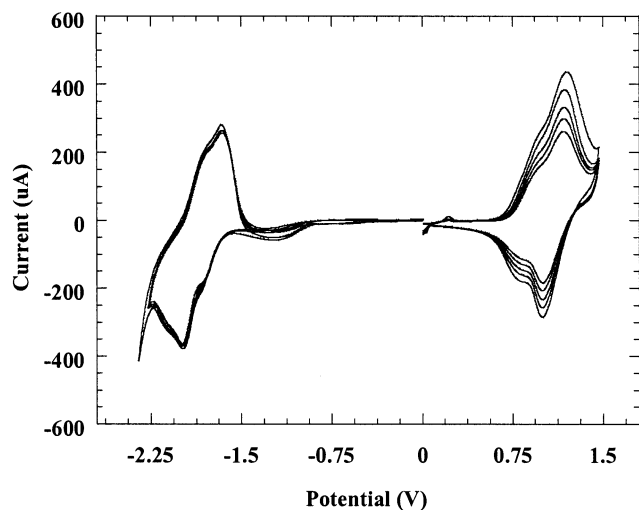
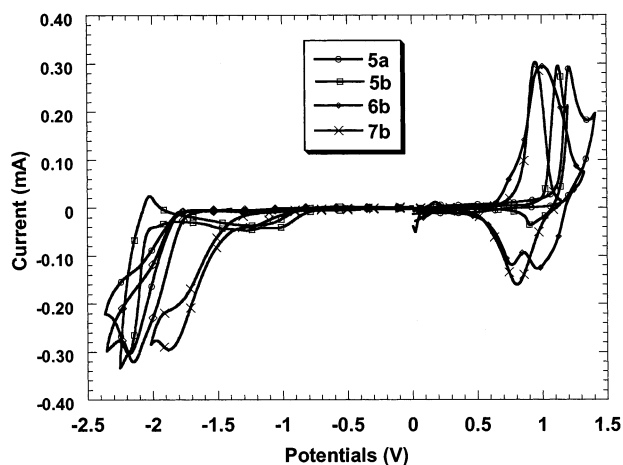**FIGURE 7.** Cyclic voltammogram of compound **3c**.

FIGURE 8. n-doping (a) and p-doping (b) cyclic voltammograms of compounds **5a**, **5b**, **6b**, and **7b**.

their corresponding poorly resolved reductive peaks were observed, which resulted from the oxidation of the dimer, radical cation, and dication. Poor reversibility of the radical cation peak indicated that it was not stable, and easily dimerized.

For the redox behavior upon cathodic scan, most of the oligothiophene-functionalized 9,9′-spirobifluorene derivatives showed very poor reversibility of the n-doping process. However, very good n-doping reversibility was observed for compounds **3b**, **3c**, and **5b**. The cyclic voltammogram of compound **3c** is given as an example in Figure 7, which shows complete reversibility of both p-doping and n-doping processes, and also has good repeatability upon multiple scans. Another trend observed from all voltammograms was that, with the oligothiophene moiety attached to the 9,9′-spirobifluorene system ranging from one thiophene ring to a trimer, the reversibility of the p-doping process was obviously improved.

The effects of varying numbers of oligothiophene substituents on the redox behaviors of the desired spiro-type molecules were also investigated. Figure 8 shows the representative p-doping and n-doping cyclic voltammograms of compounds **5a**, **5b**, **6b**, and **7b**. An obvious

cathodic shift of oxidative peak potentials was observed in the sequence of **5a**, **5b**, **6b**, and **7b**. The anodic oxidative behavior of compound **5a** onset at 1.05 V and peaked at 1.21 V, and for compound **5b** with one more thiophene unit coupled to the 7-position of the 9,9′-spirobifluorene entity in comparison with compound **5a**, the onset potential shifted to about 0.92 V and its oxidative peak shifted to 1.12 V; with the increase of the thiophene ring attached to the 9,9′-spirobifluorene system, the oxidative onset and peak potentials continually shifted to 0.80 and 1.00 V for compound **6b**, and to 0.82 and 0.94 V for compound **7b**, respectively. Of course, the peak potential of compound **7b** (0.94 V) was the lowest among these four compounds. This cathodic shift of the oxidative peak potential was due to the enhanced π-electron delocalization of the increased conjugation length, with the increase of the thiophene rings. We also observed that the oxidative potentials of nonsubstituted oligothiophene-functionalized 9,9′-spirobifluorene derivatives (from 1.69 to 0.92 V) were more sensitive to the increase of thiophene rings than those of 9,9′-spirobifluorene derivatives with *n*-hexyl groups (from 1.21 to 0.84 V). The same tendency of cathodic shift was also observed for the oxidative onset potential. In contrast, Figure 8 and Table 7 show that the increased conjugated length led to a general anodic shift for the reductive onset and peak potential. The effect of the cathodic and anodic shifts resulted in the decrease of the band gap.

We also investigated the effect of the spiro center on the electrochemical properties of oligothiophene-modified 9,9′-spirobifluorene derivatives. Electrochemical examination of various thiophene oligomers and derivatives has been done during the past decade.[20] The electrochemical properties of a series of substituted oligothiophenes and their corresponding silicon-fused oligothiophenes were also investigated.[21] The α-TMS (trimethylsilyl)-end-capped terthiophene and its silicon orthogonally fused trimer showed two oxidative peaks upon anodic scan located at 1.21 and 1.17 V, respectively.[21] For our corresponding compound **2d**, only one oxidative peak was observed with a potential of 1.45 V, which greatly shifted anodically with respect to the reported values. The same trend was found for compound **7d** in comparison with the reported corresponding septimers, which indicated that the 9,9′-spirobifluorene bridge might shift the oxidative potential anodically.

Figure 9 shows the representative n-doping and p-doping cyclic voltammograms of compounds **4a**−**d**. The influence of the different attachment patterns of thiophene oligomers to the 9,9′-spirobifluorene ring on the redox behaviors of the resulting spiro-type compounds was also investigated. On the basis of the longer singular molecular branch, compounds **4a**−**d** can be divided into two pairs, i.e., **4a** and **4c**, and **4b** and **4d**. In comarison with compounds **4a**−**c**, for compounds **4b**−**d**, the oxidative peaks shifted cathodically, while the reductive peak shifted anodically, as shown in Figure 9, which agreed with the previous demonstration of the conjugated length effect.

(20) (a) Tourillon, G.; Gourier, D.; Garnier, P.; Vivien, D. *J. Phys. Chem.* **1984**, *88*, 1049. (b) Fichou, D.; Horowitz, G.; Xu, B.; Garnier, F. *Synth. Met.* **1990**, *39*, 243.
(21) Guay, J.; Diaz, A.; Wu, R. L.; Tour, J. M. *J. Am. Chem. Soc.* **1993**, *115*, 1869.
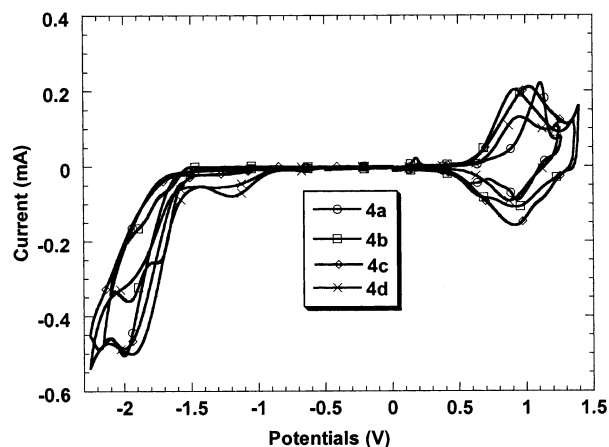
FIGURE 9. n-doping (a) and p-doping (b) cyclic voltammograms of compounds **4a**−**d**.

The data of the HOMO and LUMO energy levels of the compounds were calculated from the onset potential of p-doping and n-doping, respectively.[22] In our work, $E_{\text{HOMO}} = 4.39 + \phi_{\text{p}}'$ (eV) and $E_{\text{LUMO}} = \phi_{\text{n}}' + 4.39$ (eV), in which E_{HOMO} and E_{LUMO} mean the energy levels of the HOMO and LUMO below the vacuum. The calculated data and the band gap of 9,9′-spirobifluorene derivatives from electrochemical measurement are also summarized in Table 7. The various effects on the onset doping potentials of these 9,9′-spirobifluorene derivatives were also reflected in the variation of their HOMO and LUMO energy levels. These results demonstrated that the energy levels of the compounds depending on the oxidative onset and reductive onset could be adjusted to make them suitable for the work functions of the electrodes by varying the thiophene oligomers and their attachment patterns to the 9,9′-spirobifluorene ring.

Conclusion

In conclusion, all compounds studied exhibited good solubility in polar organic solvents, especially compounds

5a−**d** to **7a**−**d** due to the introduction of a flexible *n*-hexyl chain. All compounds studied were characterized by ^{1}H and ^{13}C NMR spectra. The results showed that a novel series of low molecular weight organic conjugated materials, oligothiophene-functionalized 9,9′-spirobifluorene derivatives, were successfully synthesized through corresponding synthetic methodologies. The chemical shifts of the protons and carbons of the 9,9′-spirobifluorene system shifted with the attachment and increase of the thiophene ring, and the bromination of thiophene rings strongly due to the electron density of protons and carbons at the thiophene ring and phenyl ring connecting with the oligothiophene ring. The thermal analysis results showed that these compounds were quite stable, and also demonstrated that these compounds could evaporate over 300 °C in place of decomposition since no more residues were observed over 700 °C. Most of the compounds exhibited a more stable amorphous glass in the solid state. The thermal stability of these materials was improved with the increase of thiophene rings. Among all derivatives, compounds **2b**, **3b**, **3d**, **4a**, and **4c** exhibited obvious crystallization and melting behavior after glass transition. In comparison with compounds **2a**−**d** to **4a**−**d**, no obvious glass transition behavior was observed for H−T regioregular oligothiophene-functionalized 9,9′-spirobifluorene derivatives (**5a**−**d** to **7a**−**d**). The electrochemical properties of all compounds studied were also investigated. The results indicated that radical cation behaviors of oligothiophene-modified 9,9′-spirobifluorene derivatives were more stable than those of normal oligothiophenes and that oxidative peak potentials shifted cathodically with the increase of the thiophene ring due to the enhanced π-delocalization of the increasing conjugation length. Oxidative potentials of oligothiophene-functionalized 9,9′-spirobifluorene derivatives were more sensitive to the increase of thiophene rings than those of 9,9′-spirobifluorene derivatives with *n*-hexyl groups. The energy band gaps of all compounds studied were also calculated from the onset potentials of n-doping and p-doping, which demonstrated that the energy levels and band gaps of these materials were easily tuned through these convenient synthetic methods.

(22) (a) Li, Y. F.; Cao, Y.; Gao, J.; Wang, D. L.; Yu, G.; Heeger, A. J. *Synth. Met.* **1999**, *99*, 243. (b) de Leeuw, D. M.; Simenon, M. M. J.; Brown, A. R.; Einerhand, R. E. F. *Synth. Met.* **1997**, *87*, 53. (c) Eckhardt, H.; Shacklette, L. W.; Jen, K. Y.; Elsenbaumer, R. L. *J. Chem. Phys.* **1989**, *91*, 1303. (d) Cervini, R.; Li, X. C.; Spencer, G. W. C.; Holmes, A. B.; Moratti, S. C.; Friend, R. H. *Synth. Met.* **1997**, *84*, 359.